

Enhanced steady-state coherences via repeated system-bath interactions

Ricardo Román-Ancheyta,^{1,*} Michal Kolář,^{2,†} Giacomo Guarneri,^{3,‡} and Radim Filip^{2,§}

¹*Instituto Nacional de Astrofísica, Óptica y Electrónica, Calle Luis Enrique Erro 1, Sta. Ma. Tonantzintla, Puebla CP 72840, México*

²*Department of Optics, Palacký University, 17. listopadu 1192/12, 771 46 Olomouc, Czech Republic*

³*School of Physics, Trinity College Dublin, College Green, Dublin 2, Ireland*

The autonomous appearance of the steady-state coherence (SSC) from system-bath interaction proves that quantum effects can appear without an external drive. Such SSC could become a resource to demonstrate quantum advantage in the applications. We predict the generation of SSC if the target system *repeatedly* interacts with independent and non-correlated bath elements. To describe the behavior of SSC, we use the collision model approach of system-bath interaction, where the system interacts with one bath element (initially in an incoherent state) at a time, asymptotically (in the fast-collision regime) mimicking a macroscopic Markovian bath coupled to the target system. Therefore, SSC qualitative behavior appears to be the same as if the continuous Markovian bath would be used. We confirm that the presence of composite system-bath interactions under the rotating-wave approximation (RWA) is the necessary condition for the generation of SSC using thermal resources in collision models. Remarkably, we show that SSC substantially increases if the target system interacts *collectively* with more than one bath element at a time. Already few bath elements collectively interacting with the target system are sufficient to increase SSC at non-zero temperatures, at the cost of tolerable lowering the final state purity.

arXiv:2008.05200v1 [quant-ph] 12 Aug 2020

* ancheyta6@gmail.com

† kolar@optics.upol.cz

‡ guarnieg@tcd.ie

§ filip@optics.upol.cz

I. INTRODUCTION

It is well known that quantum coherence is a valuable physical resource useful for many applications [1]. In quantum thermodynamics, for example, experiments have demonstrated [2] that, within the small-action limit [3], quantum coherence between different internal energy states of the working substance allows a quantum heat engine to produce more power than its classical counterpart. In quantum metrology, it has been shown [4] that long-time coherence in the state of the sensing particles can be used to outperform the precision of frequency estimation [5] when compared with entanglement-based strategies. However, such strategy relies on the coherence trapping effect [6] and, therefore, has the practical disadvantage that the state of the probes needs some initial coherence. Therefore, such quantum advantage cannot appear autonomously in quantum matter.

It is precisely the aim of several investigations to find processes in microscopic and mesoscopic systems that lead, on demand and without external coherent drives, to the generation of robust quantum coherence, entanglement in the steady-state or quantum synchronization [7]. For instance, in [8] an autonomous quantum thermal machine produces *degenerate* steady-state coherence (SSC) in a two-qubit system interacting, incoherently, with two thermal baths at different temperatures. In [9], sufficient conditions for the generation of *energetic* SSC (coherence between states with different energies [10]) in a two-level system in contact with a single thermal bath were identified. Those sufficient conditions, that we will discuss in detail in the present work, rely on the particular structure of the composite system-bath interaction. Remarkably, in both examples [8, 9], the SSC are independent of the initial state of the system, which could be initially incoherent.

The framework put forward in [9] was recently applied in [11] by obtaining non-equilibrium steady-states (NESS) with SSC. There, the thermodynamic cost to produce such coherence was calculated and, interestingly, non-zero work and heat currents at the steady-state were necessary to maintain the NESS with SSC [11]. On the other hand, in [12], an experimentally feasible semiconductor double-quantum dot charge qubit, in contact with a thermal bath, was proposed to implement the characteristic structure of the interaction Hamiltonian of [9].

In this paper, motivated by the generality of the sufficient conditions that guarantee the generation of SSC in [9], we extend those results to the framework of repeated, pulsed interactions [13–15], also known as collision models [16–20]. These models not only give theoretical insight into microscopic processes in the baths required to achieve SSC, but mainly they can be straightforwardly implemented using cold trapped ions [21] and superconducting quantum circuits [22]. Such proof-of-principle experiments will verify achievability of SSC under various conditions in parallel with the ongoing search for suitable autonomous platforms [12].

In particular, we study here the creation and *collective* enhancement of energetic SSC with (along with high purity) in a two-level system interacting with an effective heat bath. The effective heat bath is modeled as a stream of bath elements, clusters of qubits or linear harmonic oscillators in thermal states, that interact for a short period of time with the target system in which SSC is to be created. This procedure yields effectively a Markovian time-independent master equation description. We analytically solve for its steady state. For obtaining the transient dynamics we use numerical calculations, as well as approximated solutions. We find that for low-temperature heat bath, the energetic SSC of the system reaches its maximum value. This value can be substantially increased, together with the system energy, as the number of elements in the corresponding bath-clusters increases, although lowering the resulting system purity at the same time. For high bath temperatures [23], the SSC is washed out and the target system reaches a completely incoherent mixed state, irrespective of the bath-cluster size. Finally, we show that even when the composite system-bath interactions are taken into account, there exist certain scenarios in which the sufficient conditions found in [9] are not applicable for SSC generation in the context of collision models describing open quantum dynamics. This is caused by a physically different way of modelling the thermal bath in this work, compared to [9].

II. SSC FROM QUBIT BATH ELEMENTS

A. Asymptotic Coherence

In this section we focus on the setup described in Fig. 1 with individual interactions described by $N = 1$, i.e., on the case when the target system is a two-level system (TLS, qubit) with a free Hamiltonian $\mathcal{H}_S = \omega\sigma_z/2$ and the bath elements are represented by other TLS of frequency ω_B , where we have set $\hbar = 1$ from now on. We assume that the interaction between the target qubit and each respective bath element can be written in the particular form [9], allowing for spontaneous creation of steady state coherence (SSC)

$$\mathcal{V}_I = f_1\sigma_z \otimes (\sigma_-^B + \sigma_+^B) + f_2(\sigma_+ \otimes \sigma_-^B + \sigma_- \otimes \sigma_+^B), \quad (1)$$

where σ_{\pm} (σ_{\pm}^B) are the ladder operators of the target TLS (bath element) and $f_{1,2}$ are two real coupling constants. From the above expression we can identify the so called parallel, $\mathcal{H}^{\parallel\mathcal{H}_S}$, and orthogonal, $\mathcal{H}^{\perp\mathcal{H}_S} \equiv \mathcal{V}_I - \mathcal{H}^{\parallel\mathcal{H}_S}$,

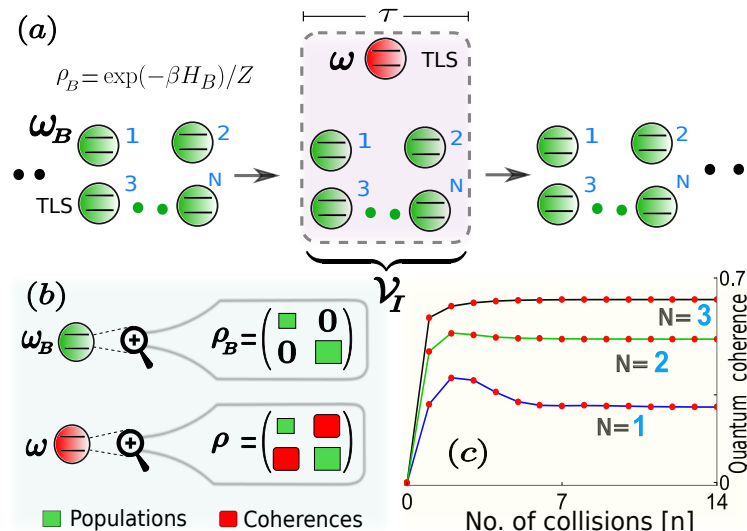


FIG. 1. Schematic representation of a basic collision model or repeated interaction scheme extended throughout the paper. **(a)** The bath elements represented by clusters of N independent and non-correlated two-level systems (TLS) or qubits (lower green circles) of frequency ω_B are initially in a thermal state of inverse temperature β . Each bath element interacts collectively during a short period of time, τ , with a target TLS (red) of the frequency ω through the interaction Hamiltonian \mathcal{V}_I . This procedure makes short-time collisions with the bath elements acting as an effective Markovian heat bath [11], although such collision-schemes have the potential to generate more general types of evolution. **(b)** Pictorial representation of the initial density matrix ρ_B of each bath TLS. Before the interaction with the target qubit ρ_B has only diagonal elements (green squares). After a few collisions, the density matrix ρ of the target TLS will contain coherence (red squares) regardless if ρ was, initially, an incoherent state. **(c)** Due to the composite structure of \mathcal{V}_I , the coherence generated in ρ reach, after several collisions, a stationary value. Remarkably, such steady-state coherence (SSC) substantially increase when the size of each cluster also increase. It is shown how fast typically SSC, quantified with the l_1 -norm of coherence, grows for $N = \{1, 2, 3\}$, $\tau = 1$ and $\beta = 5$.

components with respect to \mathcal{H}_S [9], as the first and the second term of \mathcal{V}_I , respectively. The parallel component alone ($f_1 \neq 0$, $f_2 = 0$) causes dephasing on the target qubit while creating coherence on the bath element. On the other hand, the orthogonal component alone ($f_1 = 0$, $f_2 \neq 0$) describes a damping interaction between the target system and the bath element, i.e., it causes solely quanta hopping, while the total excitation being conserved. Such hoping alone (the orthogonal part of (1)) can create coherence only between the incoherent target qubit and the incoherent bath element. Only if the bath element has quantum coherence on its own, it can be transferred to the target by the hoping interaction. In order to have non-zero quantum coherence in the target asymptotic steady-state, both interactions are therefore necessary in the interaction Hamiltonian, however, it is not clear if they are sufficient for SSC creation. Only if both components are turned on ($f_1 \cdot f_2 \neq 0$), the coherence in the bath element (created by the parallel one) are transferred to the target system by the orthogonal interaction. The interaction (1) approximately describes pulsed dynamics of two-level system in the trapped ion [21] and superconducting circuit [22] experiments when the oscillator representing bath B is weakly excited. It corresponds to the low-temperature limit, where SSC appears.

Notice that (1) can be rewritten as a bi-linear combination $\mathcal{V}_I = s^\dagger \otimes A + s \otimes A^\dagger$ between system and bath operators, if we define the operators as $s = f_1 \sigma_z + f_2 \sigma_-$ and $A = \sigma_-^B$. If we perform the corresponding trace over the incoherent bath states ρ_B , the dynamical equation for the target qubit acquires the well-known form of the following time-independent Markovian master equation (see appendix A for a detailed derivation):

$$\frac{d\rho}{dt} = -\frac{i\omega}{2} [\sigma_z, \rho] + \langle \sigma_-^B \sigma_+^B \rangle \mathcal{L}[f_1 \sigma_z + f_2 \sigma_-] \rho + \langle \sigma_+^B \sigma_-^B \rangle \mathcal{L}[f_1 \sigma_z + f_2 \sigma_+] \rho, \quad (2)$$

where $\mathcal{L}[x]\rho \equiv x\rho x^\dagger - \frac{1}{2}(x^\dagger x\rho + \rho x^\dagger x)$ is the usual Lindblad super-operator and $\langle x \rangle = \text{tr}\{x\rho_B\}$ is the expectation value of an arbitrary operator x with respect to the initial (thermal) bath state. In addition to the detailed derivation of Eq. (2) given in appendix A, we stress here that this equation holds conditioned on the limit of short interaction time τ and the condition of re-normalization of \mathcal{V}_I by $1/\sqrt{\tau}$, see appendix A for details. The above equation can be solved easily by numerical methods. Exactly the pair of above mentioned conditions allows for direct connection of the collision model and system dynamics described by an effective master equation of the Lindblad type. This connection allows for the possibility to obtain analytical expressions for $\langle \sigma_x \rangle$, $\langle \sigma_y \rangle$ and $\langle \sigma_z \rangle$, in the steady state (see appendix B). It is important to note that the second and third term in the right-hand side of (2) should not be interpreted as

terms only causing incoherent de-excitation and incoherent excitation, respectively. As we will see, these Lindblad super-operators $\mathcal{L}[x]\rho$ are able to generate coherence in the energy basis of the target qubit, even in the steady state, because they contain a linear combination of both parallel ($f_1\sigma_z$) and orthogonal ($f_2\sigma_\pm$) components with respect to \mathcal{H}_S as their argument $[x]$. We recall that for $f_1 \cdot f_2 = 0$ Eq. (2) will *not* generate SSC.

In order to quantify the possible generation of coherence in the target (qubit) system, we use the l_1 -norm of coherence measure [24]. This is defined as the absolute value of the off-diagonal element of the density matrix of interest

$$\mathcal{C}(t) = \sum_{i \neq j} |\rho_{i,j}(t)|. \quad (3)$$

For the state of the qubit ρ this can be easily written as

$$\mathcal{C}(t) = |\langle \sigma_x(t) \rangle + i \langle \sigma_y(t) \rangle|, \quad (4)$$

used from now on, having the following form in the steady-state, taking $\mathcal{C}_{\text{ss}} \equiv \lim_{t \rightarrow \infty} \mathcal{C}(t)$ (see appendix B 1 for details)

$$\mathcal{C}_{\text{ss}} = f_1 f_2 \frac{r(T)}{s(T) + \omega^2}, \quad (5)$$

where

$$r(T) = \langle [\sigma_-^B, \sigma_+^B] \rangle \sqrt{\omega^2 + \langle \{\sigma_-^B, \sigma_+^B\} \rangle^2 (2f_1^2 + f_2^2/2)^2}, \quad (6a)$$

$$s(T) = \langle \{\sigma_-^B, \sigma_+^B\} \rangle^2 (2f_1^2 + f_2^2/2)(f_1^2 + f_2^2/2), \quad (6b)$$

are two functions that, based on the result of the commutator and anti-commutator of the bath operators, may depend on the temperature T of the corresponding bath elements. For example, if each bath TLS is initially in the thermal state $\rho_{\text{th}}^B = \exp(-\beta\omega_B\sigma_z^B/2)Z^{-1}$, where $Z = 2 \cosh(\beta\omega_B/2)$ and $\beta = (k_B T)^{-1}$ is the inverse of the temperature of each bath qubit. For the specific case of bath qubits, one can always define the so called apparent temperature introduced as $T \equiv (\omega_B/k_B) \ln(p_g^B/p_e^B)^{-1}$ [23, 25], where p_g^B (p_e^B) is the probability to find each bath qubit in its ground (excited) state. Hereafter, we are going to consider a true thermal state of the bath qubits only, for the sake of simplicity. In such case $\langle [\sigma_-^B, \sigma_+^B] \rangle = \tanh(\beta\omega_B/2)$ and $\langle \{\sigma_-^B, \sigma_+^B\} \rangle = 1$. This makes $r(T)$ the only temperature dependent function. In particular, when $\beta \ll 1$ we approximate $\tanh(\beta\omega_B/2) \approx \beta\omega_B/2$ and the steady state coherence, Eq. (5), vanishes approximately as $\omega_B(\omega T)^{-1}$ in the high temperature limit. The opposite low-temperature limit, $\beta \gg 1$, leads the only thermal factor to $\tanh(\beta\omega_B/2) \approx 1$, leaving only the rest of the parameters to determine the SSC value. From Eq. (5) it is interesting to note that, as long as the product $f_1 f_2$ is different nonzero, SSC can be generated in the target qubit, even at zero temperature, see green lower curve in Fig. 2a. Ultimately, this result (5) is independent of whether we had chosen σ_y^B instead of σ_x^B as the parallel component $\mathcal{H}^{\|\mathcal{H}_S}$ of (1).

We would like to stress that the result of generation of SSC, is completely independent of the initial state of the target system and it is very different from the results obtained in [26–29]. In those works it is not possible to create SSC at zero temperature, because their strategy relies on the presence of thermal photons that must be absorbed by a composite (many-body) system made of, at least, two coupled two-level atoms (the target system) in which the SSC are to be created. Moreover, such atoms had to be close enough in space, in order to treat them as indistinguishable when a thermal photon was absorbed. This is in contrast with our repeated interaction scheme where SSC can be generated on a single two-level system.

Interestingly, following the ideas of [25, 30, 31], it is instructive to generalize previous results for the case in which the target qubit interacts, repeatedly, with *clusters* made of N independent and non-correlated bath qubits [32], instead of a single bath TLS, see Fig. 1. Thus, in Eq. (1) we can replace σ_\pm^B by $\sum_{j=1}^N \sigma_\pm^{(j)} \equiv S_\pm$ such that the corresponding collective interaction between the target qubit and each cluster looks like

$$\mathcal{V}_I = f_1 \sigma_z \otimes (S_- + S_+) + f_2 (\sigma_+ \otimes S_- + \sigma_- \otimes S_+). \quad (7)$$

The operators S_\pm are known as the collective spin operators [30]. For this new collective interaction the basic structure of (2) and (5) will essentially remain unchanged. In such case, it is easy to show that the expectation value of the commutator and anti-commutator between the collective spin operators, and with respect to the incoherent cluster state $\rho_{\text{cl}} = \bigotimes_{j=1}^N \rho_{\text{th}}^j$, ρ_{th}^j being the thermal state of the j -th qubit in the cluster, is

$$\langle \{S_-, S_+\} \rangle = N, \quad \langle [S_-, S_+] \rangle = N \tanh(\beta\omega_B/2). \quad (8)$$

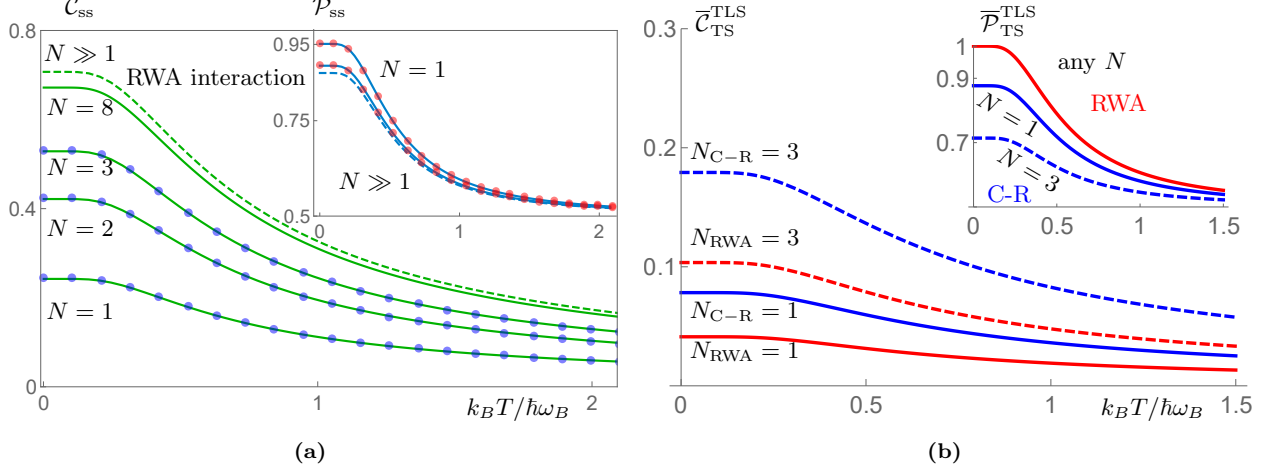


FIG. 2. (a) Steady-state coherence, SSC (5), in the target two-level system of Fig. 1 as a function of scaled temperature of the bath elements (lowest green solid line) in the case of RWA type of interaction, Eq. (7) for $N = 1$. When the target qubit interacts collectively with clusters of N non-correlated bath qubits (see Fig. 1), the SSC increases substantially (upper green solid lines) until it saturates to the value C_{ss} (green dashed line). The latter corresponds to the theoretical upper bound $C_{ss} = C_0 \tanh(\omega_B / (2k_B T))$ maximizing SSC for $N \gg 1$. Parameters are $\omega = \omega_B = 1$, $f_1 = f_2 / \sqrt{2}$, $f_2 = 0.6$ and $N = \{1, 2, 3, 8\}$. Inset: steady-state purity of the target qubit as a function of the same scaled temperature. Purity decreases when the number of qubits in the clusters increases from $N = \{1, 2\}$ (blue solid lines) until reach a saturated value (blue dashed line) when $N \gg 1$. Blue and red dots represent a purely numerical calculation of the repeated interaction model where, for $\tau = 0.051$, the steady-state is reached after $\sim 10^3$ collisions. Note that these results are independent of the initial state of the target qubit and that the C_{ss} and \mathcal{P}_{ss} have opposite trends of cluster-size N dependence. As the system coherence increases with the size of the cluster, its purity decreases. Remarkably, the plateau region in C_{ss} and \mathcal{P}_{ss} allows reaching their maximum values for $k_B T / \hbar \omega_B > 0$. (b) The dependence of optimized transient state coherence (TSC) \bar{C}_{TS} , Eq. (17), on the bath temperature in cases when the system interacts with $N = \{1, 3\}$ bath TLS via RWA interaction (labeled RWA), Eq. (7), or with counter-rotating (C-R) terms included, Eq. (13). The (C-R) results clearly have an edge over the (RWA) results in terms of attainable coherence \bar{C}_{TS} . On contrary, the corresponding optimized system state purity $\bar{\mathcal{P}}_{TS}$, Eqs. (18), of (C-R) interaction is suppressed with respect to the (RWA) scenario. The temperature dependence is entering the results through the system initial inversion $z_0 = -\tanh(\hbar\omega / (2k_B T))$ and assumption that the system and the bath have initially the same temperature T and frequency $\omega = \omega_B$. The values of the parameters are $\omega_B = \omega = 1$, $f_1 = f_2 = 0.15$. These values of the interaction constants (while being close to the edge of the validity of approximation (22)) are roughly three times smaller than the values optimizing C_{SS} in panel (a). This is the reason for lower values reached in the transient regime.

Replacing these expressions in (6a) and (6b) the l_1 -norm of coherence (5) will now also depend on N :

$$C_{ss} = f_1 f_2 \tanh(\beta \omega_B / 2) \frac{r(N)}{s(N) + \omega^2}, \quad (9)$$

where

$$r(N) = N \sqrt{\omega^2 + N^2 (2f_1^2 + f_2^2 / 2)^2}, \quad (10a)$$

$$s(N) = N^2 (2f_1^2 + f_2^2 / 2) (f_1^2 + f_2^2 / 2). \quad (10b)$$

It is worth noting that in this cluster scenario, substantial increase of the SSC values in the target qubit can be obtained when the size of each cluster also increases. The behaviour of such SSC, as a function of the bath temperature and the number of bath qubits in each cluster is shown in Fig. 2a. When the number of qubits in the clusters is large, $N \gg 1$ (upper index ∞ in Eq. (11)), the steady-state coherence (9) can be well approximated by a simple form

$$C_{ss}^\infty \approx C_0 \tanh(\beta \omega_B / 2), \quad C_0 \equiv \frac{f_1 f_2}{f_1^2 + f_2^2 / 2}, \quad (11)$$

being an upper bound for the generation of SSC at a fixed temperature, see green dashed-line of Fig. 2a. In Eq. (11), C_0 represents the l_1 -norm of coherence of the target qubit at the steady-state, at zero temperature and when N is

large, i.e., \mathcal{C}_0 is $T \rightarrow 0$ and $N \rightarrow \infty$ limit of (9). Notice that \mathcal{C}_0 as a function of f_1 or f_2 reaches an upper bound of $1/\sqrt{2} \approx 0.7$ when $f_2 = \sqrt{2}f_1$. To our best knowledge, and based on numerical evidence, this upper bound represents an absolute maximum of coherence attainable within models assumed in our work. This complements the recent numerical results obtained in [11], where the authors found that, only for $N = 1$, the maximal amount of SSC is achievable when the weights (f_1 and f_2) of the parallel and orthogonal components in (1) are equal to each other. For comparison, when a qubit is in a pure coherent superposition of energy states like $|\psi\rangle \equiv (|e\rangle + |g\rangle)/\sqrt{2}$ with $|e\rangle$ ($|g\rangle$) its excited (ground) state, the l_1 -norm of coherence of the corresponding state $\rho_\psi = |\psi\rangle\langle\psi|$ is 1, being the largest value of \mathcal{C} that one can obtain for a two-level system. Therefore, for the collision model described in Fig. 1, it is enough to have a few qubits in the incoherent clusters to generate a considerable amount of SSC (see Fig. 2a) when compared with the ideal situation of the pure coherent state $|\psi\rangle$.

To study quantum coherence in the target qubit we have chosen the energy basis of the system as our preferred basis. However, from the above results we have no indication of the qubit final state purity. The purity represents, in principle, the coherence with respect to an optimally chosen basis (achieved by a proper change of the basis) which is instructive to compare with (4). Hence, to characterize the final qubit state better, we calculate the purity $\mathcal{P}(t) = \text{tr}\{\rho^2(t)\}$ [33] which is a basis-independent quantity. The purity takes its maximum value $\mathcal{P} = 1$ if the state is pure and its minimum of $\mathcal{P} = 1/d$, with d the dimension of the corresponding Hilbert space, when the state is completely mixed [34]. For the simplest case of a density matrix of a qubit, the purity in the steady state can be easily written as $\mathcal{P}_{\text{ss}} = (1 + \mathcal{C}_{\text{ss}}^2 + \langle\sigma_z\rangle_{\text{ss}}^2)/2$, where $\langle\sigma_z\rangle_{\text{ss}}$ and \mathcal{C}_{ss} are defined in (B9) of the appendix and (9), respectively.

The inset of Fig. 2a shows the behaviour of steady-state purity \mathcal{P}_{ss} as a function of the scaled temperature of the bath qubits. We point out that for low temperatures, the final state of the target qubit is close to a pure state, especially when it interacts only with one bath qubit at a time, see Fig. 2a solid blue line. In contrast to the l_1 -norm of coherence \mathcal{C}_{ss} , the purity \mathcal{P}_{ss} decreases with the number of qubits N in each bath cluster. In particular, for $N \gg 1$ the purity in the steady state is well approximated by

$$\mathcal{P}_{\text{ss}} \approx \frac{1}{2} + \left(\frac{1}{2} + \frac{f_2^2}{8f_1^2}\right)\mathcal{C}_0^2 \tanh^2(\beta\omega_B/2). \quad (12)$$

When the second term of the above equation vanishes at high temperatures, the purity \mathcal{P}_{ss} reduces to its minimum value of 1/2, i.e., the final state of the target qubit is a completely mixed state, see blue dashed line in the inset of Fig. 2a. For any other finite value of N the purity \mathcal{P}_{ss} will fall between these two limit cases. Moreover, the plateau region in \mathcal{C}_{ss} and \mathcal{P}_{ss} allows for reaching their maximum values in the limit $0 < k_B T/\hbar\omega_B \ll 1$. In such a low-temperature regime, the purity decreases from its maximum value scales as proportional to \mathcal{C}_0^2 , i.e., is of the second order in the generated maximum coherence \mathcal{C}_0 . Remarkably, we notice a trade-off between coherence and purity for autonomous generation of SSC. In particular, relation (12) shows that the purity is a quadratic function of the SSC, cf. with Eq. (11).

It is interesting to see how the energy population of the target qubit in the steady state, measured by $\langle\sigma_z\rangle_{\text{ss}}$, is modified due to the generation of SSC. For instance, when $N \gg 1$, such expectation value is well approximated by $\langle\sigma_z\rangle_{\text{ss}} \approx -\tanh(\beta\omega_B/2)[1 - f_1\mathcal{C}_0/f_2]$, see Eq. (B9) for its exact value. This result shows that the formation of SSC induces corrections in the thermal (or bare) energy of the target qubit in case this is coupled solely to an effective thermal bath via RWA interaction, i.e., if $f_1 = 0$. In such case, the qubit population inversion is equal to the standard Boltzmann factor $2n_F - 1 = -\tanh(\beta\omega_B/2)$, where $n_F = (\exp[\hbar\omega_B/(k_B T)] + 1)^{-1}$ is the Fermi-Dirac mean occupation number of the spin system. Notice that these corrections to population are of the same order of magnitude of the SSC because they depend on f_1^2 and f_2^2 . These type of corrections were recently point it out in [12] and in the supplementary material of [9]. We additionally remark that, to get such corrections in those works, a quite complex perturbation expansion of a generalized equilibrium state has to be used for the derivation, in contrast to the simple calculations presented in our work.

So far, we have considered solely the RWA type of interaction as in Eqs. (1) and (7), including only rotating (RWA) terms in \mathcal{V}_I . However, if we want to examine the possible effects of the counter-rotating (C-R) terms included in the qubit system and the bath elements interaction Hamiltonian, we should use, e.g., the form

$$\mathcal{V}_I = f_1\sigma_z \otimes (\sigma_-^B + \sigma_+^B) + f_2(\sigma_- + \sigma_+) \otimes (\sigma_-^B + \sigma_+^B), \quad (13)$$

which can be rewritten as $\mathcal{V}_I = f_1\sigma_z \otimes \sigma_x^B + f_2\sigma_x \otimes \sigma_x^B$. This energy non-preserving interaction contains the C-R terms $\sigma_+ \otimes \sigma_+^B$ and $\sigma_- \otimes \sigma_-^B$ that were neglected in the second term of Eq. (1), reflecting the use of the RWA. Importantly, for interaction (13), we can identify the parallel and orthogonal projections $\mathcal{H}^{\parallel\mathcal{H}^s} = f_1\sigma_z \otimes \sigma_x^B$ and $\mathcal{H}^{\perp\mathcal{H}^s} = f_2\sigma_x \otimes \sigma_x^B$ respectively, again in spirit of [9]. With respect to the discussion in section III, we may alternatively refer to Eq. (13) as the Rabi-type interaction Hamiltonian. Such interaction is available in both trapped ions and superconducting circuit experiments [21, 22]. The interaction Hamiltonian (13) can be also rewritten as $\mathcal{V}_I = s^\dagger A + sA^\dagger$ with $s = f_1\sigma_z + f_2\sigma_x$

and $A = \sigma_-^B$. Here, s is a Hermitian operator, $s = s^\dagger$. Therefore, using the interaction (13) in (A7), the following master equation can be derived

$$\frac{d\rho}{dt} = -\frac{i\omega}{2}[\sigma_z, \rho] + \langle \{\sigma_-^B, \sigma_+^B\} \rangle \mathcal{L}[f_1\sigma_z + f_2\sigma_x]\rho. \quad (14)$$

In appendix (B2) we show that it is not possible to generate SSC in the target qubit if the dynamics is described by the above master equation (14). By comparison with Eq. (2) we recognize their similar structure. Up to the neglected term $f_2\sigma_-$ in the argument of the Lindbladian of Eq. (2), we can intuitively understand (14) as infinite bath temperature limit of Eq. (2), due to the equality $\langle \{\sigma_-^B, \sigma_+^B\} \rangle = \lim_{T \rightarrow \infty} \langle \sigma_+^B \sigma_-^B \rangle = 1$. Thus, the system dynamics determined by Eq. (14) will generate no coherence in the energy basis of the system in the steady-state, as it might be interpreted as $\lim_{T \rightarrow \infty} \mathcal{C}_{ss}$, see Eq. (5), and this is vanishing as T^{-1} in the high temperature limit (see discussion below Eq. (6b)).

However, it is quite remarkable that coherence in the energy basis of the target qubit can still be generated during the time evolution, see next subsection II B and also the end of appendix (B2) for details. As a matter of fact for $f_1 \cdot f_2 = 0$ Eq. (14) will not generate coherence, even in the transient evolution.

B. Optimal Transient State Coherence

In the situations considered in section II A, we have examined the qubit system properties in the “long time” (many collisions) limit. For the pulsed experimental tests [21, 22], it is advantageous to know, if the quantum coherence is attainable in the transient (finite number of collisions) regime. Such question was possible to ask in the previous work [9] as well, but there it was an extremely complex task to answer it, compared to the collision interactions used here. Therefore, we present here the results for the maximum value of coherence attainable after some specific number of collisions (for otherwise fixed values of the rest of the parameters) and its comparison to the asymptotic value of SSC. The results presented below are good approximation of the exact numerical solution in the regime of small (with respect to system frequency) values of system-bath (TLS clusters in this case) coupling constants $f_{1(2)}$.

As the coherence in the transient regime is determined by the system dynamics, one has to work out the solution of Eqs. (B2) and (B12) for the RWA approximated (RWA) interaction, cf. Eq. (7), and interaction including counter-rotating (C-R) terms, cf. Eq. (13), respectively.

These solutions read

$$\langle \vec{\sigma} \rangle^{\text{RWA}} = \exp[\mathbf{B}t](\langle \vec{\sigma} \rangle_0 + \mathbf{B}^{-1}\vec{c}) - \mathbf{B}^{-1}\vec{c}, \quad (15)$$

$$\langle \vec{\sigma} \rangle^{\text{C-R}} = \exp[\mathbb{B}t]\langle \vec{\sigma} \rangle_0, \quad (16)$$

where $\langle \vec{\sigma} \rangle_0 = (0, 0, z_0)^T$ stands for the initial Bloch vector with $z_0 = -\tanh(\beta\omega/2)$ is the inversion of the system thermal population and the superscripts RWA (C-R) reflect the type of interaction between the system qubit and the bath TLS cluster.

The derivation of the time-optimized values of coherence and purity is based on approximate solution of the above mentioned Bloch equations, using the Laplace transform method and assuming small enough damping terms in the corresponding Bloch equations, see App. B for more details. The resulting optimal values of transient state coherence (TSC) for a qubit colliding with clusters of qubits (of the size N) read

$$\begin{aligned} \bar{\mathcal{C}}_{\text{TS}}^{\text{TLS(RWA)}} &\approx 2f_1f_2N|z_0|\exp[-\pi N(f_1^2 + f_2^2/4)/\omega]/\omega, \\ \bar{\mathcal{C}}_{\text{TS}}^{\text{TLS(C-R)}} &\approx 4f_1f_2N|z_0|\exp[-\pi N(f_1^2 + f_2^2)/\omega]/\omega, \end{aligned} \quad (17)$$

being a good approximation of the exact results if the parameters satisfy $f_1, f_2 \ll \omega$, $N \lesssim 3$, and $1/2 \lesssim |z_0| \leq 1$, see horizontal gray dashed line of Fig. 6. As one can note, the transient state (TS) coherence scales with f_1, f_2 in the same way as its steady-state counterpart \mathcal{C}_{ss} in the low-temperature and weak-interaction limits. The derivation of Eqs. (17) (and (18) below) assumes that the initial system state is in thermal equilibrium with the bath and that the system is resonant with each bath element.

In the same regime of parameters, we obtain results for the optimised system purity $\bar{\mathcal{P}}$ (in the same time instant as Eq. (17)). They read

$$\begin{aligned} \bar{\mathcal{P}}_{\text{TS}}^{\text{TLS(RWA)}} &\approx \frac{1}{2}(1 + z_0^2), \\ \bar{\mathcal{P}}_{\text{TS}}^{\text{TLS(C-R)}} &\approx \frac{1}{2}(1 + z_0^2 \exp[-2\pi N(f_1^2 + f_2^2)/\omega]). \end{aligned} \quad (18)$$

The regime of parameter values, in which the above approximations work well, describes effectively the underdamped dynamics in the sense of effective system damping being weak enough. In the opposite overdamped case one should better resort to numerical evaluation.

Comparing the above results, we can see the surprising effect of the counter rotating (C-R) terms ($\sigma_+ \otimes \sigma_+^B + h.c.$) on the optimized system purity $\overline{\mathcal{P}}_{\text{TS}}^{\text{TLS(C-R)}}$ with respect to the RWA approximated $\overline{\mathcal{P}}_{\text{TS}}^{\text{TLS(RWA)}}$, whereas these terms boost the thermally generated transient state coherence $\overline{\mathcal{C}}_{\text{TS}}^{\text{TLS(C-R)}}$. The counter rotating terms result in additional basis sensitive quantum correlation of the system and the bath elements, lowering the system purity noticeably, even for the relatively short evolution times, but at the same time creating larger off-diagonal terms in the system state, see Fig. 2b. In the limit of weak damping assumed here the time at which the system coherence is maximized reads $t_{\text{max}} \approx \pi/\omega$. Although the validity range of Eqs. (17) and (18) is limited by the values below Eqs. (17), we can use numerical evidence to see that increasing the number N of the cluster units leads to monotonic increase of the coherence $\overline{\mathcal{C}}_{\text{TS}}$ and monotonic decrease of the corresponding purity $\overline{\mathcal{P}}_{\text{TS}}$, provided the rest of the parameters being fixed ($f_{1(2)} \approx 0.15$). Such feature generally holds for both types of interactions, i.e., RWA or C-R. Thorough numerical investigation of more precise quantitative behavior of the quantities of interest is beyond the scope of this paper.

In general, focusing on the TSC can be more profitable compared to SSC. The first positive aspect is the smaller number of interactions (shorter waiting time) necessary to reach the respective coherence value. Another positive aspect of TSC is that it is larger than SSC, being certainly true for C-R case, where SSC even vanishes, see discussion below Eq. (14). In the case of RWA interaction, the situation is a little bit more complex. In the small to moderate $f_{1(2)}$ values regime, c.f. Eq. (17), the TSC value always overcomes the SSC, c.f. Fig. 3a. In the regime of strong system-bath coupling, e.g., for the parameter values used in Fig. 2a, the time-optimized value of the coherence coincides with the SSC, Eq. (9).

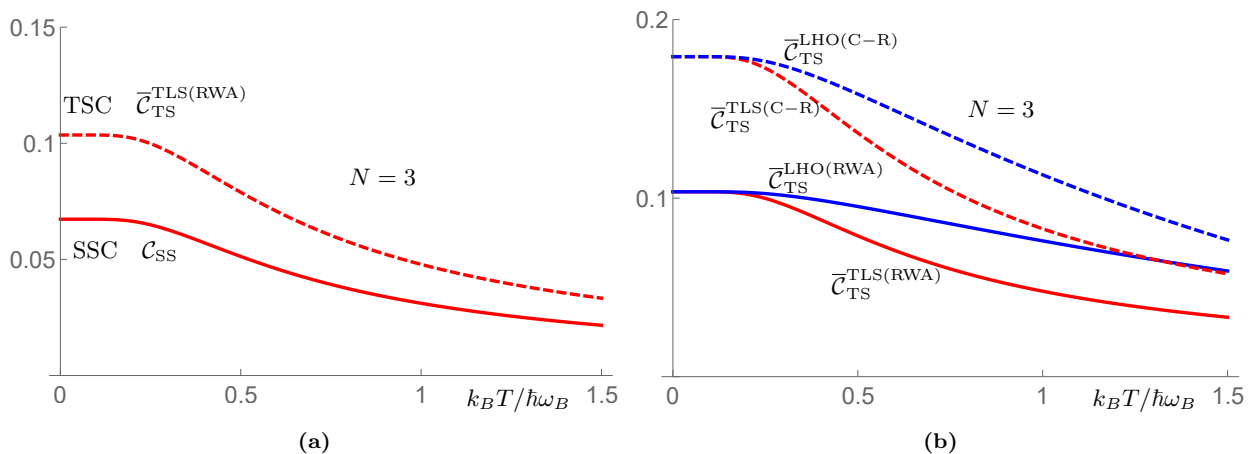


FIG. 3. (a) Comparison of the achievable coherence of the qubit interacting with clusters of $N = 3$ bath TLS and its dependence on temperature T . The figure shows the superiority and the typical behavior of the optimized TSC, Eq. (17), over the SSC, Eq. (9), for the same values of the relevant parameters, $f_1 = f_2 = 0.15$, $\omega = \omega_B = 1$, $N = 3$ in the small-to-moderate $f_{1(2)}$ regime. (b) The comparison of the optimized coherence achievable in the transient regime (TSC) with the linear harmonic oscillator (LHO) and two level system (TLS) clusters with $N = 3$ bath units and its dependence on the bath temperature T . The oscillator (LHO) clearly shows an advantage over the two level systems (TLS) in yielding higher TSC coherence for the same values of the parameters $f_1 = f_2 = 0.15$, $\omega = \omega_B = 1$, $N = 3$, c.f. Eqs. (22) and (17).

III. SSC FROM OSCILLATOR BATH ELEMENTS

A. Asymptotic Coherence

The oscillators forming bath can carry more coherence than qubits, therefore, it might be fruitful to consider an oscillator bath to generate SSC or TSC. Thus, by choosing particular composite system-bath interaction [9]

$$\mathcal{V}_I = f_1 \sigma_z \otimes (b + b^\dagger) + f_2 (\sigma_+ \otimes b + \sigma_- \otimes b^\dagger), \quad (19)$$

we assume the bath elements to be linear harmonic oscillators (LHO), instead of the two-level baths of previous section, see Fig. 4. Similarly as in the previous section II A, the coherence is at first generated in the bath but in the LHO case, the qubit cluster is not saturated and thus coherence could be expected larger, in principle, if the interaction strength f_1 increases. Formally, the interaction (19) is obtained from (1), by replacing σ_-^B (σ_+^B) with b (b^\dagger), where b (b^\dagger) is the annihilation (creation) operator of the quantum LHO such that $[b, b^\dagger] = 1$. We observe that (19) can be rewritten as $\mathcal{V}_I = s \otimes A^\dagger + s^\dagger \otimes A$ if $s = f_1 \sigma_z + f_2 \sigma_-$ and $A = b$. Therefore, it is straightforward to show that the reduced dynamics of the target qubit will be described by equation identical to (2), with the only difference that we need to replace $\langle \sigma_-^B \sigma_+^B \rangle$ by $\langle bb^\dagger \rangle$ and $\langle \sigma_+^B \sigma_-^B \rangle$ by $\langle b^\dagger b \rangle$. As in the previous section here we assume that each LHO is in a thermal state such that $\langle b^\dagger b \rangle = n_T$, $\langle \{b, b^\dagger\} \rangle = 2n_T + 1$ and $\langle [b, b^\dagger] \rangle = 1$. Here, n_T is the average Bose-Einstein occupation number given by $n_T = (\exp[\hbar\omega_B/(k_B T)] - 1)^{-1}$, whereas at high temperatures $n_T \sim k_B T/(\hbar\omega_B)$.

The interaction (19) is easily generalized, as in the previous section, to the case in which the target qubit interacts *collectively* with bath clusters made of N non-correlated and independent harmonic oscillators. For such case, the corresponding master equation describing the target qubit dynamics and its l_1 -norm of coherence in the steady-state are, basically, the same as the results (2) and (5), respectively, with the only difference that the expressions in (8) must be substituted by their bosonic counterparts

$$\langle \{B, B^\dagger\} \rangle = N \coth(\beta\omega_B/2), \quad \langle [B, B^\dagger] \rangle = N. \quad (20)$$

We have defined $B \equiv \sum_{k=1}^N b_k$ and $B^\dagger \equiv \sum_{k=1}^N b_k^\dagger$ as the collective annihilation and creation bath operators of each cluster, respectively.

To obtain the l_1 -norm of coherence in the target qubit, the expectation values (20) have to be used in Eqs. (6a) and (6b). We point out that an increase of steady-state coherence, as a function of the number of bath LHO in each cluster, is possible, see black-solid lines of Fig. 5a. It is important to mention that, although the overall behavior of the quantities plotted in Fig. 2a and Fig. 5a has similar form, it differs. For instance, in Fig. 5a the decrease of SSC with the bath temperature is slower compared to the behavior plotted in Fig. 2a. However, when the number of oscillators N within the clusters is large, the l_1 -norm of coherence in the steady-state reduces to $C_{ss} = C_0 \tanh(\beta\omega_B/2)$, which is the same limit found in previous section II A, see black dashed-line of Fig. 5a. This result can be understood in the following way, with a clear link to the results of the previous section II A. When the number N of TLSs bath elements increases, one can always use the Holstein-Primakoff representation [35] in which the collective spin operators

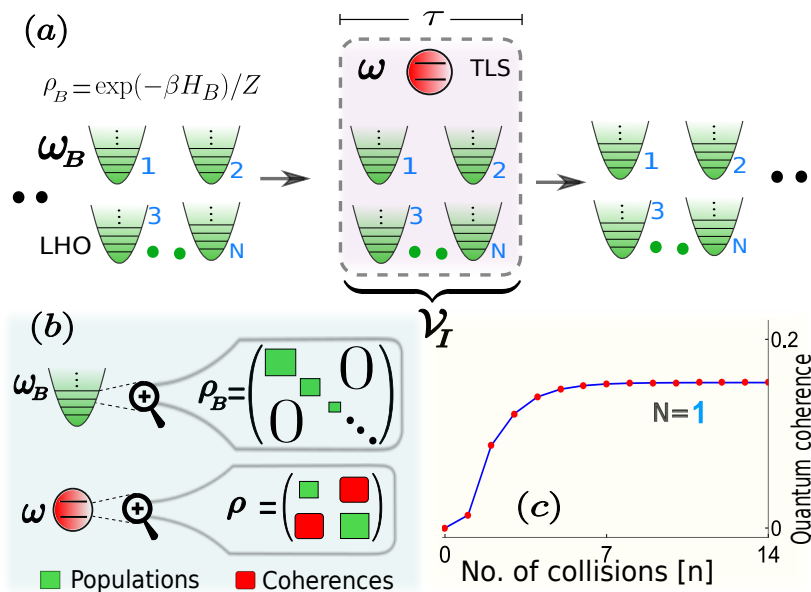


FIG. 4. (a) Schematic showing clusters of N independent and non-correlated linear harmonic oscillators (LHO) of frequency ω_B as the bath elements (green harmonic potentials) replacing the bath qubits, cf. Fig. 1. (b) Before their interaction with the target qubit (red) of frequency ω , the LHO are initially in a thermal state ρ_B where its populations (green squares) follow the standard Boltzmann distribution. After successive interactions, the density matrix ρ of the target qubit has coherence (red squares). (c) Typical behavior of the generation of SSC in the target qubit for the simplest case of $N = 1$ bath LHO in each cluster.

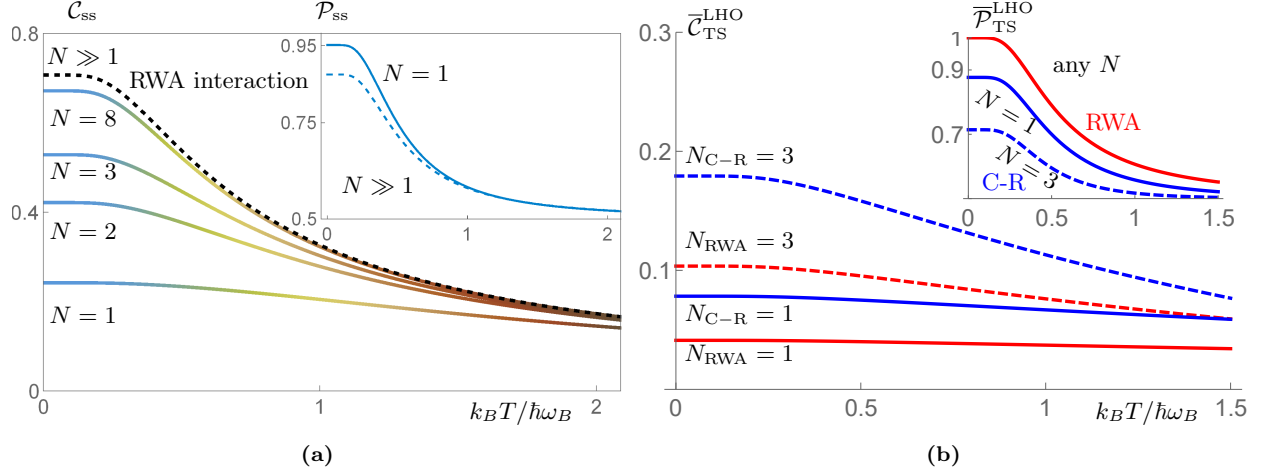


FIG. 5. (a) Steady-state coherence (SSC) with respect to the energy basis of the qubit system repeatedly colliding with the stream of LHO (representing the bath), cf. Fig. 4. As above, the coherence is quantified with the l_1 -norm of coherence, Eq. (4), as a function of the bath oscillator’s scaled temperature, see lowest solid line ($N = 1$). SSC can increase substantially if the qubit interacts with clusters of N non-correlated and independent harmonic oscillators, see upper black lines. The parameters are $\omega = \omega_B = 1$, $f_1 = f_2/\sqrt{2}$, $f_2 = 0.6$ and $N = \{1, 2, 3, 8\}$ (solid lines). The dashed-line corresponds to the theoretical limit (11) for $N \gg 1$. (b) The dependence of time-optimized coherence, Eq. (22), on the bath temperature in cases when the system interacts with $N = \{1, 3\}$ bath LHO via RWA interaction (labeled RWA), Eq. (19), or with counter-rotating (C-R) terms included, Eq. (21). As in the case of TLS bath, the (C-R) results clearly have an edge over the (RWA) results in terms of attainable coherence \bar{C} . Similarly, the corresponding system state purity $\bar{\mathcal{P}}$, Eqs. (23), of (C-R) interaction is suppressed with respect to the (RWA) scenario. The temperature dependence is entering the results through the system initial inversion $z_0 = -\tanh(\hbar\omega/(2k_B T))$ and assumption that the system and the bath have initially the same temperature T and are resonant $\omega = \omega_B$. The values of the parameters are the same as in Fig. 2b. Please note the different scales on the vertical axes on panels (a) and (b), reasons being the same as in Fig. 2b.

S_{\pm} , (7), can be written as bosonic operators in such a way that the interaction (7) and the expression of collective interaction (19) become equivalent. This procedure is sometimes called the thermodynamic limit [36], meaning that $N \rightarrow \infty$. Mathematically, this is known as the Heisenberg-Weyl contraction of the $SU(2)$ Lie group.

On the other hand, if each bath element (either harmonic oscillator or qubit) is prepared in its ground state (i.e. at zero temperature) then both $\coth(\beta\omega_B/2)$ and $\tanh(\beta\omega_B/2)$ approach unity, hence, the expectation values (20) and (8) are the same. This means that at low temperatures the target qubit reaches the same SSC values regardless if the stream of bath elements is made of harmonic oscillators or a set of qubits. This can be anticipated, because at low enough temperatures, each harmonic oscillator behaves as an effective two-level system due to the fact that there are not enough thermal excitations to populate more than the first excited state. We can therefore advantageously use bath oscillators to extended experimental platforms suitable for the tests and to obtain SSC for larger temperatures. However, for large enough bath temperatures, the C_{ss} scales approximately as ω_B/T , approaching zero as in the case of TLS bath clusters.

The inset of Fig. 5a shows the steady-state purity $\mathcal{P}_{ss} = (\langle \sigma_z \rangle_{ss}^2 + C_{ss}^2 + 1)/2$ of the target qubit at and as a function of the scaled temperature $k_B T / \hbar \omega_B$ for two limit cases, when the bath clusters are made of one harmonic oscillator (blue solid-line) and when these contain a large number $N \gg 1$ of harmonic oscillators (blue dashed-line). From the above-mentioned argument we know that the explicit expression of \mathcal{P}_{ss} , for $N \gg 1$, is given by (12). Contrary to the l_1 -norm of coherence, the purity decays faster in this configuration, compared to the case with bath qubit. This observation can be made from careful comparison of the corresponding insets of Fig. 2a and Fig. 5a. It confirms already described trade-off between the SSC and purity which rise a benchmark for further investigation of autonomous SSC.

Alternatively, we may take into account the counter-rotating terms in (19), obtaining

$$\mathcal{V}_I = f_1 \sigma_z \otimes (b + b^\dagger) + f_2 (\sigma_- + \sigma_+) \otimes (b + b^\dagger), \quad (21)$$

which resembles the interaction Hamiltonian (13). The second term of (21) is known as the quantum Rabi interaction, which is often written as $\sigma_x \otimes X_b$ [37], with $X_b \equiv b + b^\dagger$. The quantum Rabi interaction describes, in the fields of cavity and circuit quantum electrodynamics, the ultra-strong coupling regime between the electromagnetic radiation and matter at its most fundamental level [38]. To study principal appearance of SSC using the trapped ion experiments, it can be induced in a controllable way by two-tone external drive [21]. It is easy to show that the corresponding

master equation of the reduced dynamics for a target qubit, describing an interaction like (21), will be given by (14) with the replacement $\langle\{\sigma_-^B, \sigma_+^B\}\rangle \rightarrow \langle\{b, b^\dagger\}\rangle$. Therefore, no SSC can be created. The coherence occurs only during the transient dynamics governed by this master equation.

Finally, we would like to point out that we also did an analysis for the case in which we replace the target qubit, from the above scenarios, by a quantum harmonic oscillator with a free Hamiltonian $\mathcal{H}_S = \omega_0 a^\dagger a$. Remarkably, there were cases where the composite system-bath interaction having counter rotating terms could generate SSC as well. For instance, $\mathcal{V}_I = f_1 a^\dagger a \otimes X_b + f_2 X_a \otimes X_b$ and $\mathcal{V}_I = f_1 a^\dagger a \otimes \sigma_x^B + f_2 X_a \otimes \sigma_x^B$. For the first case we have the target oscillator interacting with a bath oscillator. The second case represents the inverse scenario of Fig. 4 where the role of target and the bath elements is interchanged.

B. Optimised Transient State Characteristics

As in the previous section, we compare the value of coherence and state purity generated in the steady state with the time-optimised values possible to acquire during the transient. These results reflect the experimental possibility to interrupt the evolution at certain point. We assume small $f_{1(2)}$ values case, system and bath elements to be resonant, and both in thermal initial state at temperature T .

$$\begin{aligned}\overline{\mathcal{C}}_{\text{TS}}^{\text{LHO(RWA)}} &\approx 2f_1 f_2 N \exp[-\pi N(f_1^2 + f_2^2/4)/(|z_0|\omega)]/\omega, \\ \overline{\mathcal{C}}_{\text{TS}}^{\text{LHO(C-R)}} &\approx 4f_1 f_2 N \exp[-\pi N(f_1^2 + f_2^2)/(|z_0|\omega)]/\omega,\end{aligned}\quad (22)$$

in a good approximation if the parameters satisfy $f_1, f_2 \ll \omega$, $N \lesssim 3$, and $1/2 \lesssim |z_0| \leq 1$. As in the case of TLS from the previous section, we note, that the transient state coherence (TSC) has the same scaling as its steady state (SSC) counterpart in the low-temperature and weak (in the same sense as in previous sections) coupling limits.

In the same range of parameters, we can derive the values of purity achievable at the same instant of evolution as in Eq. (22), reading

$$\begin{aligned}\overline{\mathcal{P}}_{\text{TS}}^{\text{LHO(RWA)}} &\approx \frac{1}{2} (1 + z_0^2), \\ \overline{\mathcal{P}}_{\text{TS}}^{\text{LHO(C-R)}} &\approx \frac{1}{2} (1 + z_0^2 \exp[-2\pi N(f_1^2 + f_2^2)/(|z_0|\omega)]).\end{aligned}\quad (23)$$

This difference is basically resulting from the effect of the counter rotating terms ($\sigma_+ \otimes b^\dagger + \text{h.c.}$) in the interaction Hamiltonian, present for the Rabi interaction, see Fig. 5b.

As in the previous section, see II B for details, the general comparison of the coherence achievable in TSC vs. SSC regime remains the same. The typical behavior of the system coherence when using the LHO clusters is qualitatively the same as in Fig. 3a, TSC being superior to SSC values of coherence for the same parameters in the RWA moderate interaction regime, the same being true for the C-R interaction.

At the end of this subsection, we would like to compare the results for coherence achievable with clusters of LHO vs. TLS bath units, again in the moderate coupling regime. Comparison of the results stemming from Eq. (17) and (22) shows the superiority of LHO over the TLS bath units in generating the TSC coherence, see Fig. 3b. These results imply the role of the bath units dimension in generation of the coherence in the transient dynamics and that the higher dimension of the units might be preferable for reaching higher TSC values. More thorough analysis and comparison in the strong coupling regime should rely on fully numerical approach, being beyond the scope of this paper. It will be efficient for the preparation of proof-of-principle experiment with trapped ions or superconducting circuits.

IV. CONCLUSIONS

We have shown that quantum coherence can be generated autonomously, together with high purity, on a target quantum system when this shortly interacts with individual bath elements initially in incoherent (thermal) states. The autonomous approach reaches such case without any external coherent drive or measurement performed by an external observer. In our collision (pulsed) approach, a large number of bath elements plays the role of a heat bath. Similarly to the previous work [9], based on the spin-boson model, we confirm here that composite nature of the system-bath interaction represents a necessary condition to obtain the system steady-state coherence (SSC), but on contrary not a sufficient one, as the SSC appearance depends on details of the system-bath interaction. We stress

that, unlike coherence trapping [6], the SSC is independent of the initial state of the target system. Moreover, SSC can be created on individual quantum system. This is because, from the point of view of the bath, the compound target system does not need to have parts indistinguishable like in [28, 29]. Such SSC can be increased substantially, if collective interactions between the target system and clusters of bath units are introduced. We observe that for low temperatures of the bath, the amount of SSC does not depend on the exact nature of the bath elements, both qubit or oscillator baths units reaching the same SSC value. For higher temperatures, the SSC is however higher for the oscillators-composed baths. This is of practical importance because one might have flexibility in choosing which physical systems best fit the experimental needs.

Due to the simple dynamics generated in our collision model we could study the generation of the transient coherence (TSC) in the regime of weak-to-intermediate values of the system bath coupling constants $f_{1(2)}$ in an approximate manner. Within this interaction regime we have found that for a wide range of parameters optimized TSC surpasses SSC, especially in the low-temperature regime. Moreover, in the TSC regime, it is more profitable to employ oscillator bath units than two-level system units, as well, as the former generate higher coherence of the target system.

Remarkably, the simple structure of our results also allows to characterize the intimate relationship between steady-state and transient coherence and the state purity. In particular, we have found that, for a given interaction Hamiltonian of the composite form, the coherence and purity reach their maximum in presence of a zero temperature bath, possessing a small constant plateau in the regime of small temperature (thus allowing for experimental observation) and finally show monotonic decrease for increasing temperature. It is furthermore worth noticing, however, that coherence and purity behave in the opposite way with respect to the presence of counter-rotating terms in the interaction Hamiltonian: for every fixed temperature T , the lack of these terms leads to an *increase* in the maximum achievable purity and a *decrease* in the corresponding maximum amount of coherence (where by this we mean the maximum of the SSC within the RWA approximation compared to the maximum of the TSC when counter-rotating terms are present).

Although our results show positive effects in the sense of generating relatively high SSC or TSC and purity, one may naturally ask if these results represent any fundamental limits. The answer is negative, thus the way how to beat the maximum coherence values achieved within models and settings assumed in our work can be a good future research target. Our results are of course based on our assumed models and the properties of used states, e.g., states of the bath units. Thus, if we relax some requirements on the bath-state properties, e.g., the units' independence, and we replace the bath units states by interacting (correlated), but still thermal, states we can increase the SSC and TSC values *and jointly* the system purity for otherwise the same parameters. Another way leading to possibly overcoming the limits of our current models may lie in search for more effective (in terms of coherence generation) Hamiltonians and protocols, or, e.g., in the extension of the system-bath interaction time. Such modification brings the evolution beyond the one described in our work, namely to a more complex one including terms of higher order than linear in the interaction time. Full analysis of such possible scenarios is definitely suitable topic for future work.

It may be noted that, while following from [9], in our present analysis we have focused on interactions of the system with a single bath described by the classes of system-bath interaction Hamiltonians of the form $H_{\text{int}} = \sum_j O_{s,j} \otimes b_E + h.c.$ The more general type $H_{\text{int}} = \sum_j O_{s,j} \otimes b_{E,j} + h.c.$, where the summation index is extended to the bath operators, can be considered as well (although, still describing the interaction with a single bath). Composite interactions belonging to the latter and not included in the former can, in certain cases, also lead to the generation of SSC, a recent example of which was considered in a qubit-based collision model in Eq. (30) of [11], where the presence of counter-rotating terms also allowed for the observation of SSC. While beyond the scope of the present work, this represents an interesting outlook for future work.

ACKNOWLEDGMENTS

R.R.-A. wants to thank Professor Özgür E. Müstecaplıoğlu for his hospitality at Koç University where the initial part of this work was done. R.F. and M.K. gratefully acknowledge support by the project 20-16577S of the Czech Science Foundation, LTAUSA19099 from the Czech Ministry of Education, Youth and Sports (MEYS CR) and project European Unions Horizon 2020 (20142020) research and innovation framework programme under Grant Agreement No. 731473 (project 8C18003 TheBlinQC). Project TheBlinQC has received funding from the QuantERA ERA-NET Cofund in Quantum Technologies implemented within the European Unions Horizon 2020 Programme.

Appendix A: The collision model of the system-bath interaction

This appendix describes a simple and general collision model (see an example in Fig. 1). This consists of the system of our main interest repeatedly interacting with a stream of bath elements that are initially prepared in an incoherent

state, namely the thermal state. As we show at the end of this section, a large number of the bath elements will play the role of an environment. During the short time of interaction of duration τ , the total Hamiltonian is

$$\mathcal{H} = \mathcal{H}_S + \mathcal{H}_B + \mathcal{V}_I/\sqrt{\tau}, \quad (\text{A1})$$

where \mathcal{H}_S and \mathcal{H}_B are, respectively, the system free Hamiltonian and the free Hamiltonian of one of the bath elements, and \mathcal{V}_I represents the interaction between these two. Note that, for mathematical reasons that will become clear bellow, we have rescaled the interaction term by a factor $1/\sqrt{\tau}$ [11, 13, 19, 39–41]. Apparently, shorter τ increases the interaction energy.

Further, we assume that each bath element *before* its interaction with the system of interest at a time $t_n = n\tau$, does not share any correlation with the latter and with any other bath element, so the state of the total system, $\rho_{\text{tot}}(t_n)$, is given by the tensor product between the system state denoted by $\rho(t_n)$, and a thermal state ρ_B of the incoming bath element: $\rho_{\text{tot}}(t_n) = \rho(n\tau) \otimes \rho_B$, where $\rho_B = \exp(-\beta\mathcal{H}_B)Z^{-1}$, Z is the partition function and $\beta \equiv (k_B T)^{-1}$ the inverse scaled-temperature. *After* the interaction with a bath element, the state of the system of interest at time t_{n+1} is given by the stroboscopic map [19]: $\rho[(n+1)\tau] = \text{tr}_B\{\rho'_{\text{tot}}(t_{n+1})\} \equiv \text{tr}_B\{U[\rho(n\tau) \otimes \rho_B]U^\dagger\}$, where $U = \exp(-i\mathcal{H}\tau)$ is the evolution operator of the total system and tr_B is the partial trace over the bath degrees of freedom. We can use the BakerCampbellHausdorff formula to compute the unitary transformation up to the second order in τ

$$\begin{aligned} \rho'_{\text{tot}}(t_{n+1}) &= e^{-i\mathcal{H}\tau} \rho(n\tau) \otimes \rho_B e^{i\mathcal{H}\tau} \\ &= \rho(n\tau) \otimes \rho_B - [i\mathcal{H}\tau, \rho(n\tau) \otimes \rho_B] \\ &\quad + \frac{1}{2!}[i\mathcal{H}\tau, [i\mathcal{H}\tau, \rho(n\tau) \otimes \rho_B]] + O(\tau^3), \end{aligned} \quad (\text{A2})$$

which after using (A1) in (A2) and keeping terms at most linear in τ yields

$$\begin{aligned} \rho'_{\text{tot}}(t_{n+1}) &= -i\tau[\mathcal{H}_S + \mathcal{H}_B + \mathcal{V}_I/\sqrt{\tau}, \rho(n\tau) \otimes \rho_B] \\ &\quad - \frac{\tau}{2}[\mathcal{V}_I, [\mathcal{V}_I, \rho(n\tau) \otimes \rho_B]] + \rho(n\tau) \otimes \rho_B. \end{aligned} \quad (\text{A3})$$

Taking the partial trace over the bath B in the above expression and without any loss of generality assuming $\text{tr}_B\{\mathcal{V}_I\rho_B\} = 0$, as customary [17, 19, 42, 43], we get

$$\begin{aligned} \rho((n+1)\tau) - \rho(n\tau) &= -i\tau[\mathcal{H}_S, \rho(n\tau)] \\ &\quad - \frac{\tau}{2}\text{tr}_B\{[\mathcal{V}_I, [\mathcal{V}_I, \rho(n\tau) \otimes \rho_B]]\}, \end{aligned} \quad (\text{A4})$$

which does not depend on the free bath Hamiltonian \mathcal{H}_B . The condition $\text{tr}_B\{\mathcal{V}_I\rho_B\} = 0$ does not restrict the interaction with the bath elements, actually, such assumption can be enforced by moving into the interaction picture representation of a rescaled local Hamiltonian of the system, see [42, 43]. For a particular example where $\text{tr}_B\{\mathcal{V}_I\rho_B\} \neq 0$ and its impact on the spectral response of the target system see Ref. [25]. Then, the continuous-time limit of the model can be obtained if we divide (A4) by τ and take the limit $\tau \rightarrow 0$ [16, 18, 25, 30, 31]. This yields the reduced dynamics of the qubit density matrix as [13, 19, 41]

$$\frac{d\rho}{dt} = -i[\mathcal{H}_S, \rho] - \frac{1}{2}\text{tr}_B\{[\mathcal{V}_I, [\mathcal{V}_I, \rho \otimes \rho_B]]\}, \quad (\text{A5})$$

where $d\rho/dt \equiv \lim_{\tau \rightarrow 0}[\rho((n+1)\tau) - \rho(n\tau)]\tau^{-1}$.

For the case in which \mathcal{V}_I can be written as the bi-linear combination $\mathcal{V}_I = s^\dagger A + s A^\dagger$ between system and bath operators, s and A respectively, the bath trace in (A5) can be easily worked out. Thus, with such an interaction Hamiltonian, Eq. (A5) acquires simple and more familiar Lindblad form:

$$\frac{d\rho}{dt} = -i[\mathcal{H}_S, \rho] + \langle AA^\dagger \rangle \mathcal{L}[s]\rho + \langle A^\dagger A \rangle \mathcal{L}[s^\dagger]\rho, \quad (\text{A6})$$

where $\mathcal{L}[x]\rho \equiv x\rho x^\dagger - \frac{1}{2}(x^\dagger x\rho + \rho x^\dagger x)$ and $\langle x \rangle \equiv \text{tr}\{x\rho_B\}$ with ρ_B being the initial (thermal) state of the bath. Using (1) as the interaction Hamiltonian in (A6) we obtain Eq. (2) of the main text. Let us point out that, for the special case in which s is a Hermitian operator, $s = s^\dagger$, Eq. (A6) reduces to

$$\frac{d\rho}{dt} = -i[\mathcal{H}_S, \rho] + \langle \{A, A^\dagger\} \rangle \mathcal{L}[s]\rho, \quad (\text{A7})$$

where $\{x, x^\dagger\} = xx^\dagger + x^\dagger x$ is the anti-commutator. In section II we can see that (A6) and (A7) are useful master equations describing, respectively, system-bath interactions with and without the rotating wave approximation.

Appendix B: Bloch equations and steady state coherence

1. Rotating-wave-approximated interactions

Here we describe how to derive equation (5) of the main text using the interaction (1) with the counter-rotating terms neglected (RWA performed). First, we should note that from Eq. (2) it is easy to prove, after some algebra, the following identities:

$$\begin{aligned} \text{tr}\{\mathcal{L}[f_1\sigma_z + f_2\sigma_{\pm}]\rho\sigma_x\} &= -\left(2f_1^2 + \frac{f_2^2}{2}\right)\langle\sigma_x\rangle \\ &\quad + f_1f_2\langle\sigma_z\rangle \mp f_1f_2, \end{aligned} \quad (\text{B1a})$$

$$\text{tr}\{\mathcal{L}[f_1\sigma_z + f_2\sigma_{\pm}]\rho\sigma_y\} = -\left(2f_1^2 + \frac{f_2^2}{2}\right)\langle\sigma_y\rangle, \quad (\text{B1b})$$

$$\text{tr}\{\mathcal{L}[f_1\sigma_z + f_2\sigma_{\pm}]\rho\sigma_z\} = -f_2^2\langle\sigma_z\rangle + f_1f_2\langle\sigma_x\rangle \pm f_2^2. \quad (\text{B1c})$$

These identities will be useful to calculate the expectation values $\langle\sigma_i\rangle$, where $i = \{x, y, z\}$, with respect to the state ρ of the target qubit. Defining the vectors $\vec{\sigma} = (\sigma_x, \sigma_y, \sigma_z)^\top$ and $\vec{c} = (c_x, 0, -c_z)^\top$ and using Eq. (2) along with the above expressions, the corresponding Bloch equations can be written as:

$$\frac{d}{dt}\langle\vec{\sigma}\rangle = \mathbf{B}\langle\vec{\sigma}\rangle + \vec{c}, \quad (\text{B2})$$

where $\langle\vec{\sigma}\rangle$ is the Bloch vector and \mathbf{B} is the following matrix

$$\mathbf{B} = \begin{pmatrix} -\Gamma & -\omega & \Omega \\ \omega & -\Gamma & 0 \\ \Omega & 0 & -\gamma \end{pmatrix}. \quad (\text{B3})$$

These Bloch equations follow directly from the quantum master equation (A7), without any further approximation or additional assumptions. We have defined the matrix elements of \mathbf{B} as:

$$\gamma = f_2^2\langle\{\sigma_-^B, \sigma_+^B\}\rangle, \quad c_x = 2(f_1/f_2)c_z, \quad (\text{B4})$$

$$\Omega = f_1f_2\langle\{\sigma_-^B, \sigma_+^B\}\rangle, \quad c_z = f_2^2\langle[\sigma_-^B, \sigma_+^B]\rangle, \quad (\text{B5})$$

$$\Gamma = (2f_1^2 + f_2^2/2)\langle\{\sigma_-^B, \sigma_+^B\}\rangle, \quad (\text{B6})$$

with averaging done with respect to ρ_B , the initial (thermal) state of the bath. Making $d\langle\vec{\sigma}\rangle/dt = 0$ the steady-state values $\langle\sigma_i\rangle_{\text{ss}}$ of (B2) are easily obtained:

$$\langle\sigma_x\rangle_{\text{ss}} = \frac{f_1f_2\langle[\sigma_-^B, \sigma_+^B]\rangle\Gamma}{\Gamma^2 + \omega^2 - (f_1/f_2)^2\gamma\Gamma}, \quad (\text{B7})$$

$$\langle\sigma_y\rangle_{\text{ss}} = \frac{\omega}{\Gamma}\langle\sigma_x\rangle_{\text{ss}}, \quad (\text{B8})$$

$$\langle\sigma_z\rangle_{\text{ss}} = \frac{\Omega}{\gamma}\langle\sigma_x\rangle_{\text{ss}} - \frac{c_z}{\gamma}. \quad (\text{B9})$$

To quantify the generation of SSC in the state ρ of the target qubit we use the l_1 -norm of coherence, which is a suitable measure to compute it [24]. For a two-level system this can be defined as $\mathcal{C}(t) = |\langle\sigma_x(t)\rangle + i\langle\sigma_y(t)\rangle|$. At the steady state, and using (B8), it reduces to

$$\mathcal{C}_{\text{ss}} = \langle\sigma_x\rangle_{\text{ss}}\sqrt{1 + \left(\frac{\omega}{\Gamma}\right)^2}. \quad (\text{B10})$$

When we substitute (B6) and (B7) in the above expression we obtain Eq. (5) of the main text. Evidently, all these results are easily generalized for the case in which the stream of bath single qubits are replaced for a stream of bath clusters that interact with the target qubit (see Fig. 1). In such case, we should replace the commutator and anti-commutator for their respective expressions given by Eq. (8) of the main text.

2. Beyond-RWA interactions

Here we derive the steady-state solution of the Bloch vector when the master equation (14) of the main text is used to describe the dynamics of the target qubit, i.e., when counter-rotating (C-R) terms like the ones in (13) are taken into account. Using part of the second term in the right hand side of (14) we can calculate the following quantities:

$$\text{tr}\{\mathcal{L}[f_1\sigma_z + f_2\sigma_x]\rho\sigma_x\} = -2f_1^2\langle\sigma_x\rangle + 2f_1f_2\langle\sigma_z\rangle, \quad (\text{B11a})$$

$$\text{tr}\{\mathcal{L}[f_1\sigma_z + f_2\sigma_x]\rho\sigma_y\} = -2(f_1^2 + f_2^2)\langle\sigma_y\rangle, \quad (\text{B11b})$$

$$\text{tr}\{\mathcal{L}[f_1\sigma_z + f_2\sigma_x]\rho\sigma_z\} = -2f_2^2\langle\sigma_z\rangle + 2f_1f_2\langle\sigma_x\rangle. \quad (\text{B11c})$$

We take these expressions to write the corresponding Bloch equations:

$$\frac{d\langle\vec{\sigma}\rangle}{dt} = \mathbb{B}\langle\vec{\sigma}\rangle, \quad (\text{B12})$$

where $\vec{\sigma} = (\sigma_x, \sigma_y, \sigma_z)^\top$ and

$$\mathbb{B} = \begin{pmatrix} -\gamma_\phi & -\omega & \Omega \\ \omega & -(\gamma_\phi + \gamma) & 0 \\ \Omega & 0 & -\gamma \end{pmatrix}. \quad (\text{B13})$$

Note that the following definitions have been used: $\gamma_\phi = 2f_1^2\langle\{\sigma_-^B, \sigma_+^B\}\rangle$, $\gamma = 2f_2^2\langle\{\sigma_-^B, \sigma_+^B\}\rangle$ and $\Omega = 2f_1f_2\langle\{\sigma_-^B, \sigma_+^B\}\rangle$. From (B12) we can interpret γ_ϕ as an effective dephasing rate, γ as an effective decay rate and Ω can be seen as an effective pumping term. The equation (B12) is a homogeneous one, without any driving term inducing energy population or quantum coherence.

It is easy to check that the steady-state solution of the Bloch vector is $\langle\vec{\sigma}\rangle_{\text{ss}} = (0, 0, 0)^\top$. This means that the target qubit probe ends up into a mix state with equal probabilities. Therefore, no steady-state coherences can be generated in the qubit probe when Rabi-type of interactions are considered as the orthogonal part of the system Hamiltonian. However, during the time evolution or transient, it is still possible to show that a certain amount of coherences in the target qubit can be generated. To see this, using the Laplace transform method, we obtain the following approximated solutions for each component of the Bloch vector

$$\langle\sigma_x(t)\rangle \approx \frac{z_0\Omega \exp(-3\gamma_\phi t/2)}{\sqrt{\omega^2 - \Omega^2 - \gamma_\phi^2/4}} \sin\left(t\sqrt{\omega^2 - \Omega^2 - \gamma_\phi^2/4}\right), \quad (\text{B14})$$

$$\langle\sigma_y(t)\rangle \approx \frac{z_0\Omega\omega \exp(-2\gamma_\phi t)}{\omega^2 - \Omega^2} \left[1 - \cos\left(t\sqrt{\omega^2 - \Omega^2}\right)\right], \quad (\text{B15})$$

$$\langle\sigma_z(t)\rangle \approx \frac{\Omega}{\omega}\langle\sigma_y(t)\rangle + z_0 \exp(-2\gamma_\phi t), \quad (\text{B16})$$

where $z_0 = \langle\sigma_z(0)\rangle$ and $\langle\sigma_x(0)\rangle = \langle\sigma_y(0)\rangle = 0$ are the initial conditions of $\langle\vec{\sigma}\rangle$. The above expressions were obtained under the assumption $\gamma \approx 2\gamma_\phi$, corresponding to the choice of the values of coupling constants $f_2 = \sqrt{2}f_1$. Additionally to this condition, we have made the approximation $3\gamma_\phi \approx 2\gamma_\phi$, by assuming small coupling values f_1, f_2 with respect to ω . Therefore, (B14-B16) will be a good approximated solution of the Bloch vector if all these requirements are satisfied, see an example in Fig. 6. These assumptions suggest that the more general form of the exponential arguments within these approximations is $\exp[-t(\gamma + \gamma_\phi)/2]$. To obtain results allowing for time optimized values of \overline{C}_{TS} and $\overline{\mathcal{P}}_{\text{TS}}$, we neglect γ_ϕ and Ω with respect to ω in arguments of goniometric functions in Eqs. (B14), yielding

$$\langle\sigma_x(t)\rangle \approx \frac{z_0\Omega \exp[-t(\gamma + \gamma_\phi)/2]}{\omega} \sin(t\omega), \quad (\text{B17})$$

$$\langle\sigma_y(t)\rangle \approx \frac{z_0\Omega \exp[-t(\gamma + \gamma_\phi)/2]}{\omega} [1 - \cos(t\omega)], \quad (\text{B18})$$

$$\langle\sigma_z(t)\rangle \approx z_0 \exp[-t(\gamma + \gamma_\phi)/2]. \quad (\text{B19})$$

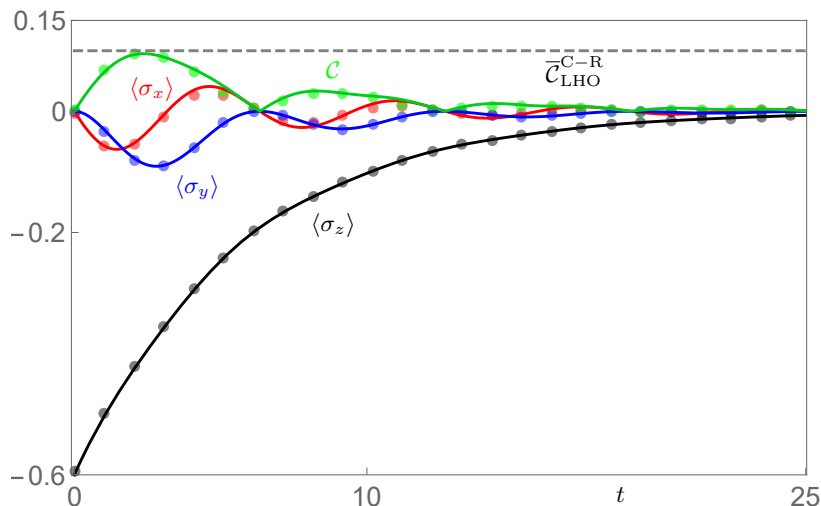


FIG. 6. Approximate evolution for the components of the Bloch vector: $\langle \sigma_x \rangle$ (red line), $\langle \sigma_y \rangle$ (blue line) and $\langle \sigma_z \rangle$ (black line). The green line is the l_1 -norm of coherence C and the black dashed line is the optimized maximum according to Eq. (22). We have set $\sqrt{2}f_1 = f_2$, $f_2 = 0.3$. The initial state of the qubit probe is a mixed state such that $\langle \sigma_z(0) \rangle = -0.6$. Results from an exact numerical simulation of the repeated (collision) interactions are shown as the tick opacity dots, where the time between each collision is set to $\tau = 0.051$.

Such simplified time evolution allows for time-optimization of the coherence $C \equiv |\langle \sigma_x(t) \rangle + i\langle \sigma_y(t) \rangle|$ and purity $\mathcal{P} \equiv (1 + |\langle \vec{\sigma} \rangle|^2)/2$, yielding Eqs. (17)-(22) and Eqs. (18)-(23). These results represent in fact weakly damped oscillations of the Bloch vector in the regime of small system-bath coupling constants $f_{1(2)}$.

The optimization procedure has the same ground in the case of RWA interaction, Eq. (19), only the intermediate results are more cumbersome.

-
- [1] Alexander Streltsov, Gerardo Adesso, and Martin B. Plenio, “Colloquium: Quantum coherence as a resource,” *Rev. Mod. Phys.* **89**, 041003 (2017).
 - [2] James Klatzow, Jonas N. Becker, Patrick M. Ledingham, Christian Weinzetl, Krzysztof T. Kaczmarek, Dylan J. Saunders, Joshua Nunn, Ian A. Walmsley, Raam Uzdin, and Eilon Poem, “Experimental demonstration of quantum effects in the operation of microscopic heat engines,” *Phys. Rev. Lett.* **122**, 110601 (2019).
 - [3] Raam Uzdin, Amikam Levy, and Ronnie Kosloff, “Equivalence of quantum heat machines, and quantum-thermodynamic signatures,” *Phys. Rev. X* **5**, 031044 (2015).
 - [4] A Smirne, A Lemmer, M B Plenio, and S F Huelga, “Improving the precision of frequency estimation via long-time coherences,” *Quantum Science and Technology* **4**, 025004 (2019).
 - [5] Andrea Smirne, Jan Kołodyński, Susana F. Huelga, and Rafał Demkowicz-Dobrzański, “Ultimate precision limits for noisy frequency estimation,” *Phys. Rev. Lett.* **116**, 120801 (2016).
 - [6] Carole Addis, Gregoire Brebner, Pinja Haikka, and Sabrina Maniscalco, “Coherence trapping and information backflow in dephasing qubits,” *Phys. Rev. A* **89**, 024101 (2014).
 - [7] Goktug Karpat, Iskender Yalçınkaya, and Barış Çakmak, “Quantum synchronization in a collision model,” *Phys. Rev. A* **100**, 012133 (2019).
 - [8] Jonatan Bohr Brask, Géraldine Haack, Nicolas Brunner, and Marcus Huber, “Autonomous quantum thermal machine for generating steady-state entanglement,” *New Journal of Physics* **17**, 113029 (2015).
 - [9] Giacomo Guarneri, Michal Kolář, and Radim Filip, “Steady-state coherences by composite system-bath interactions,” *Phys. Rev. Lett.* **121**, 070401 (2018).
 - [10] Gonzalo Manzano, Ralph Silva, and Juan M. R. Parrondo, “Autonomous thermal machine for amplification and control of energetic coherence,” *Phys. Rev. E* **99**, 042135 (2019).
 - [11] Giacomo Guarneri, Daniele Morrone, Barış Çakmak, Francesco Plastina, and Steve Campbell, “Non-equilibrium steady-states of memoryless quantum collision models,” *Physics Letters A*, 126576 (2020).
 - [12] Archak Purkayastha, Giacomo Guarneri, Mark T. Mitchison, Radim Filip, and John Goold, “Tunable phonon-induced steady-state coherence in a double-quantum-dot charge qubit,” *npj Quantum Information* **6**, 27 (2020).
 - [13] Philipp Strasberg, Gernot Schaller, Tobias Brandes, and Massimiliano Esposito, “Quantum and information thermodynamics: A unifying framework based on repeated interactions,” *Phys. Rev. X* **7**, 021003 (2017).

- [14] Philipp Strasberg, “Repeated interactions and quantum stochastic thermodynamics at strong coupling,” *Phys. Rev. Lett.* **123**, 180604 (2019).
- [15] Stella Seah, Stefan Nimmrichter, and Valerio Scarani, “Nonequilibrium dynamics with finite-time repeated interactions,” *Phys. Rev. E* **99**, 042103 (2019).
- [16] F. Ciccarello, G. M. Palma, and V. Giovannetti, “Collision-model-based approach to non-markovian quantum dynamics,” *Phys. Rev. A* **87**, 040103 (2013).
- [17] Salvatore Lorenzo, Francesco Ciccarello, and G. Massimo Palma, “Composite quantum collision models,” *Phys. Rev. A* **96**, 032107 (2017).
- [18] Francesco Ciccarello, “Collision models in quantum optics,” *Quantum Measurements and Quantum Metrology* **4**, 53–63 (2017).
- [19] Franklin L. S. Rodrigues, Gabriele De Chiara, Mauro Paternostro, and Gabriel T. Landi, “Thermodynamics of weakly coherent collisional models,” *Phys. Rev. Lett.* **123**, 140601 (2019).
- [20] Onur Pusuluk and Özgür E Müstecaplıođlu, “Thermocoherent effect: heat currents driven by quantum coherence and correlations,” arXiv preprint arXiv:2006.03186 (2020).
- [21] C. Flhmann, T. L. Nguyen, M. Marinelli, V. Negnevitsky, K. Mehta, and J. P. Home, “Encoding a qubit in a trapped-ion mechanical oscillator,” *Nature* **566**, 513–517 (2019).
- [22] P. Campagne-Ibarcq, A. Eickbusch, S. Touzard, E. Zalys-Geller, N. E. Frattini, V. V. Sivak, P. Reinhold, S. Puri, S. Shankar, R. J. Schoelkopf, L. Frunzio, M. Mirrahimi, and M. H. Devoret, “Quantum error correction of a qubit encoded in grid states of an oscillator,” arXiv (2019), 1907.12487 [quant-ph].
- [23] C L Latune, I Sinayskiy, and F Petruccione, “Apparent temperature: demystifying the relation between quantum coherence, correlations, and heat flows,” *Quantum Science and Technology* **4**, 025005 (2019).
- [24] T. Baumgratz, M. Cramer, and M. B. Plenio, “Quantifying coherence,” *Phys. Rev. Lett.* **113**, 140401 (2014).
- [25] Ricardo Román-Ancheyta, Barış Çakmak, and Özgür E Müstecaplıođlu, “Spectral signatures of non-thermal baths in quantum thermalization,” *Quantum Science and Technology* **5**, 015003 (2020).
- [26] B. Çakmak, A. Manatuly, and Ö. E. Müstecaplıođlu, “Thermal production, protection, and heat exchange of quantum coherences,” *Phys. Rev. A* **96**, 032117 (2017).
- [27] Barış Çakmak, “Ergotropy from coherences in an open quantum system,” arXiv preprint arXiv:2005.08489 (2020).
- [28] C. L. Latune, I. Sinayskiy, and F. Petruccione, “Energetic and entropic effects of bath-induced coherences,” *Phys. Rev. A* **99**, 052105 (2019).
- [29] C. L. Latune, I. Sinayskiy, and F. Petruccione, “Thermodynamics from indistinguishability: Mitigating and amplifying the effects of the bath,” *Phys. Rev. Research* **1**, 033192 (2019).
- [30] Angsar Manatuly, Wolfgang Niedenzu, Ricardo Román-Ancheyta, Barış Çakmak, Özgür E. Müstecaplıođlu, and Gershon Kurizki, “Collectively enhanced thermalization via multiqubit collisions,” *Phys. Rev. E* **99**, 042145 (2019).
- [31] Deniz Türkcpe and Ricardo Román-Ancheyta, “Tailoring the thermalization time of a cavity field using distinct atomic reservoirs,” *J. Opt. Soc. Am. B* **36**, 1252–1259 (2019).
- [32] D. A. Gangloff, G. Éthier-Majcher, C. Lang, E. V. Denning, J. H. Bodey, D. M. Jackson, E. Clarke, M. Hugues, C. Le Gall, and M. Atatüre, “Quantum interface of an electron and a nuclear ensemble,” *Science* **364**, 62–66 (2019).
- [33] Michael A Nielsen and Isaac Chuang, *Quantum computation and quantum information* (Cambridge University Press Cambridge, 2002).
- [34] Carlos A. González-Gutiérrez, Ricardo Román-Ancheyta, Diego Espitia, and Rosario Lo Franco, “Relations between entanglement and purity in non-markovian dynamics,” *International Journal of Quantum Information* **14**, 1650031 (2016).
- [35] Masashi Ban, “Decomposition formulas for $su(1, 1)$ and $su(2)$ lie algebras and their applications in quantum optics,” *J. Opt. Soc. Am. B* **10**, 1347–1359 (1993).
- [36] Jorge G. Hirsch, Octavio Castaos, Ramn Lpez-Pea, and Eduardo Nahmad-Achar, “Mean field description of the Dicke model,” *AIP Conference Proceedings* **1424**, 144–148 (2012), <https://aip.scitation.org/doi/pdf/10.1063/1.3688964>.
- [37] P. Forn-Díaz, L. Lamata, E. Rico, J. Kono, and E. Solano, “Ultrastrong coupling regimes of light-matter interaction,” *Rev. Mod. Phys.* **91**, 025005 (2019).
- [38] Anton Frisk Kockum, Adam Miranowicz, Simone De Liberato, Salvatore Savasta, and Franco Nori, “Ultrastrong coupling between light and matter,” *Nature Reviews Physics* **1**, 19–40 (2019).
- [39] Dragi Karevski and Thierry Platini, “Quantum nonequilibrium steady states induced by repeated interactions,” *Phys. Rev. Lett.* **102**, 207207 (2009).
- [40] Gabriel T. Landi, E. Novais, Mário J. de Oliveira, and Dragi Karevski, “Flux rectification in the quantum xxz chain,” *Phys. Rev. E* **90**, 042142 (2014).
- [41] Gabriele De Chiara, Gabriel Landi, Adam Hewgill, Brendan Reid, Alessandro Ferraro, Augusto J Roncaglia, and Mauro Antezza, “Reconciliation of quantum local master equations with thermodynamics,” *New Journal of Physics* **20**, 113024 (2018).
- [42] V. Giovannetti and G. M. Palma, “Master equations for correlated quantum channels,” *Phys. Rev. Lett.* **108**, 040401 (2012).
- [43] Ángel Rivas and Susana F. Huelga, “Microscopic description: Markovian case,” in *Open Quantum Systems: An Introduction* (Springer Berlin Heidelberg, Berlin, Heidelberg, 2012) pp. 49–80.